

Contents lists available at ScienceDirect

Journal of the Mechanics and Physics of Solids

journal homepage: www.elsevier.com/locate/jmps





I too $\bigvee I_2$: A new class of hyperelastic isotropic incompressible models based solely on the second invariant

Ellen Kuhl a,1, Alain Goriely b,*,1

- ^a Department of Mechanical Engineering, Stanford University, Stanford, CA 94305, United States
- ^b Mathematical Institute, University of Oxford, Oxford, UK

ARTICLE INFO

Keywords: Elasticity Constitutive modeling Soft tissues Poynting effect Invariants

ABSTRACT

In contemporary elasticity theory, the strain–energy function predominantly relies on the first invariant I_1 of the deformation tensor; a practice that has been influenced by models derived from rubber elasticity. However, this approach may not fully capture the complexities of materials exhibiting pronounced shear deformations, such as very soft biological tissues. Here, we explore the implications and potential benefits of constitutive models where the strain–energy function is exclusively a function of the second invariant, I_2 . By shifting the focus towards I_2 , we aim to address the limitations of current models in accurately describing shear-dominated behaviors and to provide a more comprehensive understanding of material responses, particularly for materials that do not conform to the assumptions underlying I_1 -centric theories. Through theoretical musings, data analysis, and automated model discovery, we investigate the feasibility of this approach and its consequences for predicting material behavior under various loading conditions. We show that the so-called "second-invariant materials" conforming to I_2 -only have interesting properties that are found in biological tissues and are fundamentally different from the traditional "first-invariant materials".

1. Introduction

In the field of elasticity, constitutive modeling plays a pivotal role in our ability to predict material response under various loads. The core of such modeling lies in the formulation of strain–energy functions, which are scalar fields representing the stored energy per unit volume in a material. To accurately describe the mechanical behavior of such *hyperelastic* materials, these functions have traditionally been constructed from the invariants of the deformation tensor. These invariants are unique scalar quantities that remain unchanged under any coordinate transformation, thus providing an objective measure of deformation. The primary invariants typically employed for isotropic materials are the first, second, and third invariants of the left Cauchy–Green deformation tensor. By leveraging these invariants, constitutive models can encapsulate the material's response to external forces or deformations and ensure that the stress–strain relationships are framed in an invariant manner, satisfying both material objectivity and the laws of thermodynamics (Ogden, 1984; Fu and Ogden, 2001). This invariant-based approach forms the foundation of hyperelastic material modeling, offering a rigorous and robust framework for simulating the complex behavior of materials under mechanical loads.

In this context, it is well appreciated that the second invariant of the strain tensor, I_2 , represents an underutilized yet significant component in the theoretical framework of elasticity (Horgan and Smayda, 2012; Anssari-Benam et al., 2021). Despite its fundamental role in characterizing the deformation state of a material, particularly in describing the shape changes that are

E-mail address: goriely@maths.ox.ac.uk (A. Goriely).

https://doi.org/10.1016/j.jmps.2024.105670

Received 18 March 2024; Received in revised form 19 April 2024; Accepted 26 April 2024 Available online 3 May 2024

^{*} Corresponding author.

¹ Both authors have contributed equally to this work.

independent of volume change, I_2 has not been sufficiently integrated into elasticity theory and its applications (Alibakhshi et al., 2021). This oversight may stem from the historical focus on simpler deformation models or analytical challenges in incorporating I_2 into existing frameworks. However, the inclusion of I_2 is crucial for a more comprehensive understanding of material behavior, especially in describing the properties of biological soft tissues under complex loading scenarios where deformations cannot be accurately described by the first invariant I_1 alone.

Exploring a theory of elasticity primarily focused on the second invariant presents a compelling new research direction, particularly for addressing the mechanical behavior of very soft biological materials, for example from the brain or arteries. These materials exhibit complex mechanical properties that traditional elasticity theories, which predominantly concentrate on the first invariant may not adequately capture. For instance, many such materials exhibit the reverse Poynting effect (Mihai and Goriely, 2011, 2012). Therefore, the distinctive deformation characteristics of soft biological tissues, marked by pronounced shape changes with minimal volume change, highlight the relevance of I_2 in accurately describing their mechanical responses, especially under shear (Destrade et al., 2012).

While many authors have emphasized the need to include the second invariant to obtain a better characterization of a material, here we go one step further and consider the consequences of a theory based *solely* on the second invariant. The reason for this choice is twofold. First, the systematic system identification of data sets for a variety of samples leads to the puzzling finding, against all common practice, that some materials are better represented by a strain–energy functions that only depend on I_2 . Second, by taking the limit to I_2 -only materials theoretically, we can gain a better understanding of the effect of the second invariant on the properties of tissues and improve our understanding of isotropic incompressible hyperelastic materials.

2. Background and definitions

We consider a solid subject to a deformation $\mathbf{x} = \chi(\mathbf{X})$, which maps material points \mathbf{X} in the reference configuration to points \mathbf{x} in the current configuration (see Ogden (1984), Goriely (2017) for reference and notation). Then the deformation gradient tensor, that measures changes between the two configurations is

$$\mathbf{F} = \operatorname{Grad}(\chi),\tag{1}$$

where Grad() is the gradient with respect to the reference coordinates. The left Cauchy–Green deformation tensor B is related to the deformation gradient tensor by $B = FF^{\mathsf{T}}$, where F^{T} is the transpose of F. This tensor characterizes the local deformation of the material and is used to define the invariants of deformation, which are scalar quantities invariant under coordinate transformations. The principal invariants of B are:

$$I_1 = \operatorname{tr}(\mathbf{B}),\tag{2}$$

$$I_2 = \frac{1}{2} \left[(\text{tr}(\mathbf{B}))^2 - \text{tr}(\mathbf{B}^2) \right], \tag{3}$$

$$I_3 = \det(\mathbf{B}),\tag{4}$$

where tr(B) is the trace of B, and det(B) is the determinant of B.

These invariants can also be expressed in terms of the *principal stretches* $\{\lambda_1, \lambda_2, \lambda_3\}$ which are the square roots of the eigenvalues of **B**:

$$I_1 = \lambda_1^2 + \lambda_2^2 + \lambda_3^2, \tag{5}$$

$$I_2 = \lambda_1^2 \lambda_2^2 + \lambda_2^2 \lambda_3^2 + \lambda_1^2 \lambda_3^2, \tag{6}$$

$$I_3 = \lambda_1^2 \lambda_2^2 \lambda_3^2. (7)$$

In the particular case when the motion is *isochoric*, $I_3 = 1$, and the second invariant can also be written as $I_2 = \lambda_1^{-2} + \lambda_2^{-2} + \lambda_3^{-2}$.

2.1. Geometric interpretation of the three invariants

The invariants are not only algebraic objects that emerge from the analysis of the strain tensors, they also have a natural geometric interpretation (Aydogdu et al., 2021; Kearsley, 1989; Miehe et al., 2004).

We start with the easy one, the third invariant of the deformation tensor, I_3 , which measures the relative volume change of a material element during deformation. If I_3 is greater than 1, the material element has expanded, and if I_3 is less than 1, it has contracted. Hence, I_3 provides a scalar measure of the volumetric dilation or compression of a material element due to deformation.

It is also relatively easy to interpret the first invariant of the deformation tensor, I_1 . Geometrically, I_1 represents the sum of the squared stretches of an infinitesimal line element averaged over all possible orientations within the material. In the classical theory of rubber elasticity, this mechanism to store energy is particularly relevant as it simplifies the complex molecular chain network of rubber into a single scalar quantity that represents the average stretch between crosslinks in the network. The averaging process inherent to I_1 allows for the consideration of stretches in all directions, providing a scalar measure of deformation that is a fundamental building block for all constitutive models of isotropic hyperelastic materials that are based on the elongation of molecular chains.

The second invariant, I_2 , is harder to interpret. Nevertheless, it can be shown that it gives three times the square of the stretch ratio of an infinitesimal area element averaged over all possible orientations (Kearsley, 1989). Therefore, this invariant takes into account

changes in shape that an area element undergoes during deformation. To compute I_2 , one can consider an infinitesimal area oriented in a Cartesian coordinate system that undergoes deformation. I_2 captures the average of the product of any two distinct stretches in that plane across all orientations. Therefore, this averaging process considers the area element's orientations in the deformed state and quantifies the extent of shear deformation which makes I_2 particularly relevant in the analysis of materials that undergo large shear deformations.

2.2. Constitutive models

The strain-energy function W is a scalar function that quantifies the elastic energy stored in a material due to deformation. For isotropic hyperelastic materials, W is solely a function of the three strain invariants $W = W(I_1, I_2, I_3)$. In the case of incompressible materials, such as rubber, the volume is conserved during deformation, implying $I_3 = 1$. For such materials, the strain-energy function can be simplified to depend only on I_1 and I_2 , as $W = W(I_1, I_2)$.

The Cauchy stress tensor T can be derived from the strain–energy function for an isotropic incompressible hyperelastic material using the well-known representation formula:

$$\mathbf{T} = -p\mathbf{1} + 2W_1\mathbf{B} - 2W_2\mathbf{B}^{-1},\tag{8}$$

where p is the Lagrange multiplier enforcing the incompressibility constraint, $det(\mathbf{F}) = 1$, and 1 the identity tensor. We have also introduced the notation

$$W_1 = \frac{\partial W}{\partial I_1}, \quad W_2 = \frac{\partial W}{\partial I_2}. \tag{9}$$

In the absence of body forces, the equilibrium of the material is described by

$$\operatorname{div} \mathbf{T} = \mathbf{0},\tag{10}$$

where div() is the divergence operator with respect to x, ensuring that the net force on any part of the material vanishes. The determination of the appropriate form of W is a central problem in the theory of elasticity since there is no general theory that provides its functional form based on first principles. Different choices for W lead to quantitative and qualitative differences in the material response.

The starting point of most studies is the *neo-Hookean model*. It offers a simple yet powerful description of the elastic behavior of elastomeric materials at finite deformation. It is simply given by

$$W = C_1[I_1 - 3], (11)$$

where $C_1 = E/6$ is related to the small-strain Young's modulus E. This modulus can be connected to molecular-level phenomena, thus allowing the macroscopic mechanical properties to be related to the microstructure of the material (Beatty, 2003).

The first-invariant model (FIM) (also known as the generalized neo-Hookean model) extends this concept by imposing that W depends only on the first invariant I_1 which simplifies both the choice of possible functional forms and hence model fitting, as well as the mathematical treatment of these materials. However, this choice also implies a focus on the compressive and tensile material behaviors and assumes a microscopic model based on affine deformations. It implies that energy is stored only in chain extension and compression (Ehret and Stracuzzi, 2022).

In contrast, the *Mooney–Rivlin model* (Mooney, 1940; Rivlin, 1948), was one of the first to incorporate I_2 -dependent terms, which significantly improved the agreement between theory and experiments. It is given by a linear combination of the first and second invariants,

$$W = C_1[I_1 - 3] + C_2[I_2 - 3], \tag{12}$$

and allows for a more accurate characterization of shear deformations, which are particularly important in incompressible soft materials. The constants C_1 and C_2 are material constants determined empirically to fit the experimental data. From a microstructural point of view, the introduction of I_2 reflects contributions of chain interactions when they are constrained within a tube-like region around the molecular chains (Fried, 2002). Indeed it was shown that micromechanical models that include an area stretch induced by tube-like domains lead to macroscale continuum models with strong I_2 dependence (Kumar and Brassart, 2023) and, similarly, that the addition of an energy penalty term for changes in tube area is best fitted, at the macroscopic level, by an extra dependence in I_2 (Puglisi and Saccomandi, 2016).

3. Theoretical considerations

3.1. The second-invariant model

Here, in contrast to the classical approach of introducing the second invariant, I_2 , as a means to improve the data fit of a first-invariant model, we consider the extreme case of materials that *only* depend on I_2 , that we refer to, for lack of a better name, as the *second-invariant model* (SIM):

$$W = w(I_2), (13)$$

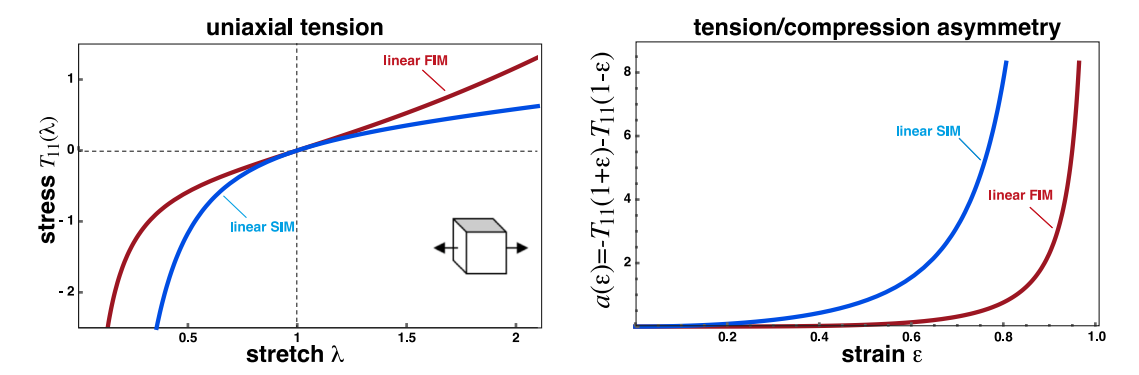


Fig. 1. Uniaxial tension and asymmetry between compression and tension. Left: Tension versus stretch for the linear FIM (red) and linear SIM (blue), showing that for the same Young's modulus, the linear SIM model is softer in extension and stiffer in compression than the corresponding FIM. Right: The asymmetry coefficient as a function of the strain shows a much larger asymmetry for the linear SIM.

the simplest one of which is the linear SIM, $W = C_2[I_2-3]$, which was first introduced by Hill in 1973 under the name extreme-Mooney material. For these materials, Hill showed that there are new exact solutions that can be expressed in terms of Bessel functions (Hill, 1973). The only other isotropic material that does not include I_1 is the Blatz-Ko model originally introduced to describe elastomeric foams (Blatz and Ko, 1962).

3.2. Homogeneous deformations

3.2.1. Uniaxial tension and compression

Simple extension refers to a deformation applied to a material, where a uniaxial load is exerted along one principal axis, typically elongating the material in that direction while contracting it in the perpendicular directions due to the Poisson effect. This deformation is characterized by a stretch ratio, λ , where $\lambda > 1$ denotes uniaxial tension and $\lambda < 1$ denotes uniaxial compression. In the context of a rectangular block, this deformation can be described by

$$x_1 = \lambda X_1, \quad x_2 = \lambda^{-1/2} X_2, \quad x_3 = \lambda^{-1/2} X_3,$$
 (14)

where, as before, x_i and X_i represent the coordinates in the deformed and reference configurations. For this mode of deformation, we have

$$I_1 = \lambda^2 + \frac{2}{\lambda}, \qquad I_2 = \frac{1}{\lambda^2} + 2\lambda,$$
 (15)

and the axial stress is

$$T_{11} = 2\left(\lambda^2 - \frac{1}{\lambda}\right)\left(W_1 + \frac{W_2}{\lambda}\right). \tag{16}$$

Therefore, for SIMs we have

$$T_{11} = 2w'(I_2)(\lambda - \frac{1}{\lambda^2}). \tag{17}$$

Close to the undeformed reference state, $\lambda = 1$, we recover a Hookean behavior by linearizing this law with a Young's modulus given by

$$E = \left. \frac{\partial T_{11}}{\partial \lambda} \right|_{\lambda=1} = 6w'(3). \tag{18}$$

Interestingly, for the linear law, we obtain the simple relationship $E = 6C_2$, and conclude that we can describe a Hookean behavior without any dependence on the first invariant I_1 .

It is of interest to compare the asymmetric behavior in tension and compression between FIMs and SIMs. Starting with the linear case, we compare the two models by imposing that they have the same linear behavior close to the undeformed state, $\lambda = 1$ in Fig. 1. To illustrate the asymmetry between tension and compression, we also display the asymmetry coefficient

$$a(\epsilon) = -T_{11}(1+\epsilon) - T_{11}(1-\epsilon), \tag{19}$$

and conclude that the linear SIM displays a much stronger asymmetry than the neo-Hookean model. This asymmetry between tension and compression is also present in the general models. Indeed, a series expansion around $\lambda = 1$ reveals the following behavior for any FIM and SIM:

$$T_{11}^{\text{FIM}} = -E(\lambda - 1) + \mathcal{O}((\lambda - 1)^3), \qquad a^{\text{FIM}} = 0 + \mathcal{O}(\epsilon^3), \tag{20}$$

$$T_{11}^{\text{FIM}} = -E(\lambda - 1) + \mathcal{O}((\lambda - 1)^3), \qquad a^{\text{FIM}} = 0 + \mathcal{O}(\epsilon^3),$$

$$T_{11}^{\text{SIM}} = -E(\lambda - 1) - E(\lambda - 1)^2 + \mathcal{O}((\lambda - 1)^3), \qquad a^{\text{SIM}} = 2E\epsilon^2 + \mathcal{O}(\epsilon^3),$$
(21)

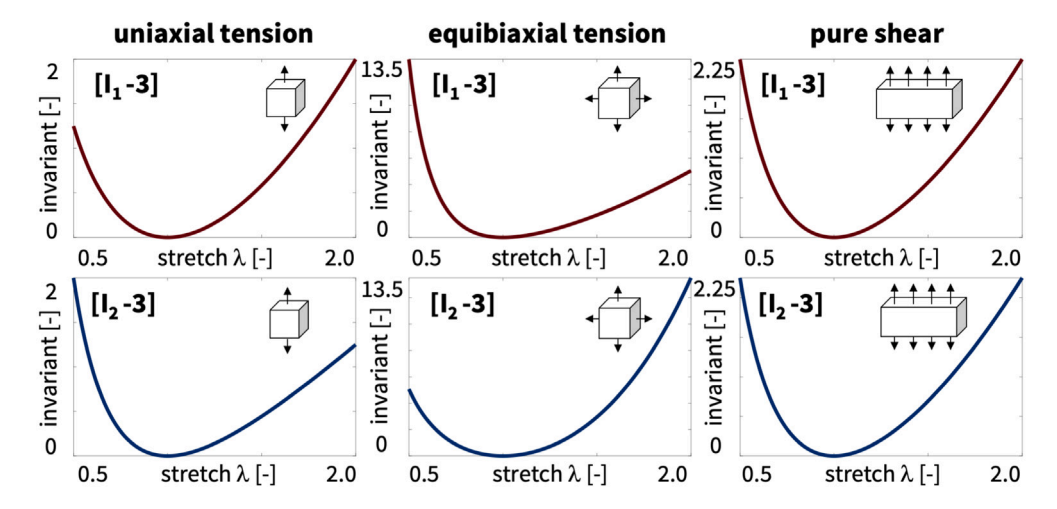


Fig. 2. Invariants as functions of stretch. First invariant I_1 , top row, and second invariant I_2 , bottom row, as functions of the stretch λ for the homogeneous deformations of uniaxial tension, equibiaxial tension, and pure shear. Both invariants display tension/compression asymmetry. For the special case of pure shear, both invariants are identical.

from which we conclude that SIMs are better suited to describe materials with a strong asymmetry between tension and compression as found in soft tissues, see Section 4.

3.2.2. Triaxial deformations

Triaxial homogeneous deformations are characterized by an independent and uniform stretch along three mutually perpendicular axes, usually corresponding to the principal material directions. Explicitly, these deformations are described by the stretches λ_1 , λ_2 , λ_3 along the X_1 , X_2 , and X_3 axes, respectively:

$$x_1 = \lambda_1 X_1, \ x_2 = \lambda_2 X_2, \ x_3 = \lambda_3 X_3.$$
 (22)

For such deformations, the invariants are:

$$I_1 = \lambda_1^2 + \lambda_2^2 + \lambda_3^2, \qquad I_2 = \lambda_1^{-2} + \lambda_2^{-2} + \lambda_3^{-2}.$$
 (23)

The Cauchy stress tensor is then diagonal with components:

$$T_{11} = 2(\lambda_1^2 - \lambda_2^2)(W_1 + \lambda_1^2 W_2), \qquad T_{22} = 2(\lambda_2^2 - \lambda_2^2)(W_1 + \lambda_2^2 W_2). \tag{24}$$

For SIMs, the ratio of these two stresses provides a new universal relation (Beatty, 1987; Pucci and Saccomandi, 1997; Saccomandi, 2001):

$$\frac{T_{11}}{T_{22}} = \frac{\lambda_2^2 \left(\lambda_1^2 - \lambda_3^2\right)}{\lambda_1^2 \left(\lambda_2^2 - \lambda_3^2\right)}.$$
 (25)

Since this relation does not explicitly depend on the choice of $w = w(I_2)$, it can be used to test if the material is indeed modeled by a SIM, independently of the functional form of w.

Apart from uniaxial extension, there are two more interesting special cases of triaxial deformations. First, *biaxial extension* is obtained by taking $\lambda_1 = \lambda_2 = \lambda$. Second, the case where $\lambda_1 = 1$, $\lambda_2 = \lambda > 1$ and $\lambda_3 = 1/\lambda$ is sometimes called *pure shear* (Treloar, 1944) as an applied traction in the vertical direction must be compensated by a stress in the horizontal direction.

We can summarize the behavior of FIMs and SIMs for triaxial deformations by comparing the profile of the invariants and stretches as a function of a single parameter in these three typical cases, as shown in Figs. 2 and 3.

From Fig. 2 we see that both invariants display tension compression asymmetry. Interestingly, for the special case of incompressibility with $I_1 = \lambda_1^2 + \lambda_2^2 + \lambda_2^2$ and $I_2 = \lambda_1^{-2} + \lambda_2^{-2} + \lambda_2^{-2}$, in the range $1/2 \le \lambda \le 2$, the minima and maxima of the first and second invariants are identical, but for the special cases of uniaxial and equibiaxial tension, they occur under tension versus compression. For the special case of pure shear, both invariants are identical.

Fig. 3 illustrates the stress as a function of the stretch for different choices of strain-energy functions. The first and second rows display the stresses for FIMs and SIMs for the examples of a linear, $W = [I_{1,2}-3]$, exponential linear, $W = \exp([I_{1,2}-3])-1$, quadratic, $W = [I_{1,2}-3]^2$, and exponential quadratic, $W = \exp([I_{1,2}-3]^2)-1$, strain-energy function. While the four functions are identical for both invariants for the special case of pure shear, they clearly differ under uniaxial and equibiaxial tension. This suggests that materials that display strong first-invariant characteristics cannot be modeled accurately with second invariant models, and vice versa. While the linear and quadratic terms, $W = [I_{1,2}-3]$ and $W = [I_{1,2}-3]^2$, generally capture a smooth increase of the stress with increasing stretch, the exponential linear and exponential quadratic terms, $W = \exp([I_{1,2}-3])-1$ and $W = \exp([I_{1,2}-3]^2)-1$,

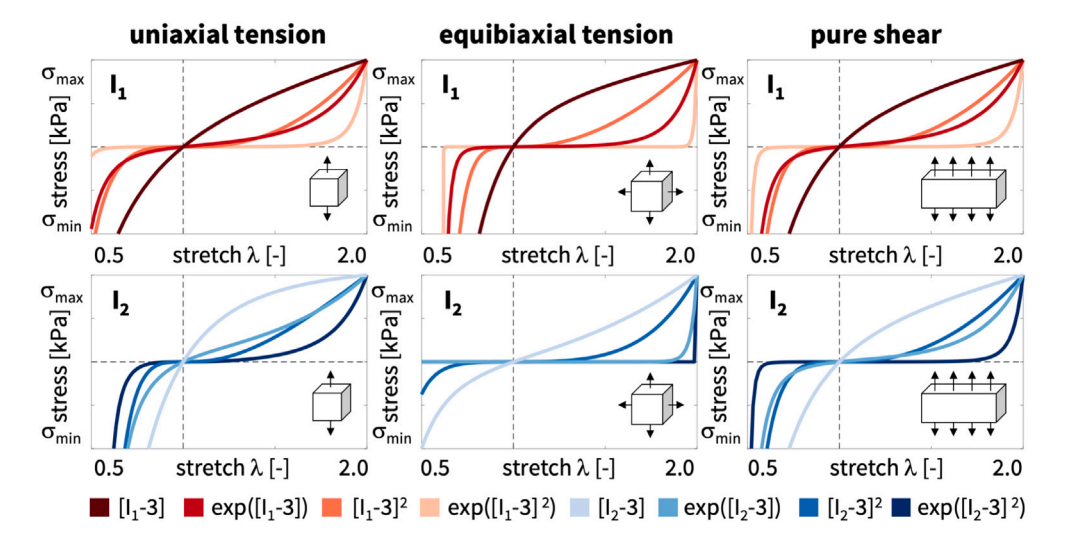


Fig. 3. Stresses as functions of stretch. Stress components related to the first invariant I_1 , top row, and second invariant I_2 , bottom row, as functions of the stretch λ for the homogeneous deformations of uniaxial tension, equibiaxial tension, and pure shear. All stresses display tension compression asymmetry. For the special case of pure shear, the stress components are identical.

display a steep increase and are good candidate terms to characterize strain hardening that arises from limited microstructural chain extensibility. Notably, the quadratic functions, $W = [I_{1,2} - 3]^2$ and $W = \exp([I_{1,2} - 3]^2) - 1$, have horizontal tangents at the origin leading to zero Young's modulus and, when used alone without any additional terms, may result in complications, for example, in finite element analyses. We also note that both FIMs and SIMs can exhibit strain-hardening. Using a Gent-like energy function with a vertical asymptote for a SIM is also possible but a careful justification about the implication of a limiting value of I_2 in terms of micromechanical model would be needed.

3.2.3. Simple shear

Simple shear is an isochoric (i.e. volume-preserving) deformation, commonly used in the experimental characterization and theoretical study of material behavior. It is given by the deformation

$$x_1 = X_1 + kX_2, \ x_2 = X_2, \ x_3 = X_3,$$
 (26)

where k represents the shear magnitude in the $X_1 - X_2$ plane, with the shear angle given by $\arctan(k)$. This deformation does not change the volume because it involves a sliding motion of material planes over one another without altering the distance between these planes along the X_3 axis. The deformation gradient is:

$$\mathbf{F} = \begin{bmatrix} 1 & k & 0 \\ 0 & 1 & 0 \\ 0 & 0 & 1 \end{bmatrix},\tag{27}$$

and is such that I_1 and I_2 are identical, $I_1 = I_2 = 3 + k^2$. The Cauchy stress tensor for simple shear is given by

$$\mathbf{T} = \begin{bmatrix} 2k^2W_1 & 2k(W_1 + W_2) & 0\\ 2k(W_1 + W_2) & -2k^2W_2 & 0\\ 0 & 0 & 0 \end{bmatrix}.$$
 (28)

We note that, since the two invariants are equal, a data set purely generated from simple shear testing (and hence providing only T_{12}) can be fitted equally by a FIM or a SIM. Without additional data on the loadings or different loading modes that exhibit a difference between the two invariants, there is no possibility of distinguishing the two models. For SIMs, the stress simplifies to

$$\mathbf{T} = \begin{bmatrix} 0 & 2kW_2 & 0\\ 2kW_2 & -2k^2W_2 & 0\\ 0 & 0 & 0 \end{bmatrix},\tag{29}$$

the implication of which will become clear shortly. We note that one can choose W_2 to obtain shear softening. For instance, we can start with a FIM which is either a sum or arbitrary powers of I_1 as proposed in Lopez-Pamies (2010) or the logarithmic form proposed in Anssari-Benam and Horgan (2021, 2022) and replace I_1 by I_2 to fit the shear data (albeit, it will not match the same tension data since $I_1 \neq I_2$ in tension).

3.2.4. Ideal shear

Confusingly, pure shear has two different definitions. Hence, to avoid confusion, we discuss here a deformation that we refer to as *ideal shear* with the unavoidable caveat that some authors describe it as pure shear (Moon and Truesdell, 1974). It is defined by a Cauchy stress tensor **T**, in Cartesian coordinates, of the form:

$$[\mathbf{T}] = \begin{bmatrix} 0 & T & 0 \\ T & 0 & 0 \\ 0 & 0 & 0 \end{bmatrix},\tag{30}$$

where T is the magnitude of the shear stress acting in the $x_1 - x_2$ plane. It corresponds to the deformation

$$x_1 = aX_1 + \sqrt{b^2 - a^2}X_2, \ x_2 = bX_2, \ x_3 = cX_3,$$
 (31)

where a, b, and c depend on the material model and are chosen such that abc = 1 for incompressibility. The shear stress is related to the deformation through:

$$T = 2b\sqrt{b^2 - a^2} \left(W_1 + W_2 \frac{1}{a^2 b^2} \right). \tag{32}$$

3.3. Inhomogeneous deformations

Finally, it is instructive to see how materials described by SIMs respond for non-homogeneous deformations. Here we consider the example of the classical torsion problem (Goriely, 2017, p. 333) where a long solid circular cylinder of radius A is subjected to a torsional deformation. Using cylindrical coordinates, where (R, Θ, Z) represents the position of a material point in the undeformed configuration and (r, θ, z) represents the same point in deformed configuration, the deformation is given by

$$r = R, \ \theta = \Theta + \tau Z, \ z = Z,$$
 (33)

where τ is the twist per unit length. The Cauchy stress resulting from this torsional deformation is

$$\mathbf{T} = T_{rr}\mathbf{e}_r \otimes \mathbf{e}_r + T_{\theta\theta}\mathbf{e}_{\theta} \otimes \mathbf{e}_{\theta} + T_{zz}\mathbf{e}_z \otimes \mathbf{e}_z + T_{z\theta}\mathbf{e}_z \otimes \mathbf{e}_{\theta}, \tag{34}$$

where

$$T_{rr} = -\tau^2 \int_{R}^{A} r W_1(r) dr,$$
 (35)

$$T_{\theta\theta} = -2\tau^2 \int_{R}^{A} rW_1(r)dr + 2\tau^2 R^2 W_1,$$
(36)

$$T_{zz} = -\tau^2 \int_R^A r W_1(s) dr - 2\tau^2 R^2 W_2,$$
(37)

$$T_{z\theta} = 2\tau R(W_1 + W_2),$$
 (38)

where W_1 and W_2 are evaluated for the torsion problem at $I_1 = I_2 = 3 + \tau^2 R^2$.

The resultant moment M and axial force N required to maintain the deformation are determined by integrating the shear stress $T_{z\theta}$ and axial stress T_{zz} over the cross-sectional area of the cylinder, yielding:

$$M = \int_0^{2\pi} \int_0^A T_{z\theta} R^2 dR d\Theta = 4\pi\tau \int_0^A R^3 (W_1 + W_2) dR,$$
 (39)

$$N = \int_{0}^{2\pi} \int_{0}^{A} T_{zz} R \, \mathrm{d}R \mathrm{d}\Theta = -2\pi \tau^{2} \int_{0}^{A} R^{3} (W_{1} + 2W_{2}) \mathrm{d}R. \tag{40}$$

For SIMs, it follows that $N = -\tau M$. We also note the particularly simple form of the stress

$$T_{rr} = T_{\theta\theta} = 0, \ T_{zz} = -2\tau^2 R^2 W_2, \ T_{z\theta} = 2\tau R W_2,$$
 (41)

which leads to another universal relation

$$T_{z\theta} = -\tau R T_{zz}. (42)$$

We also conclude from (41) that no pressure develops on the side of the cylinder as it is twisted (which corresponds to the absence of lateral traction T_{11} during simple shear).

3.4. Adscititious inequalities

In the absence of a systematic way to obtain strain–energy functions from first principles, we are restricted to general principles that must be guaranteed to satisfy plausible behaviors (Truesdell and Noll, 2004). For instance, we recall that a fundamental set of such inequalities are the Baker-Ericksen inequalities:

$$\lambda_i \neq \lambda_i \Rightarrow (t_i - t_i)(\lambda_i - \lambda_i) > 0, \quad \text{for } i, j = 1, 2, 3,$$

where $\{t_1, t_2, t_3\}$ represent the principal stresses, the eigenvalues of **T**, and, as before, $\{\lambda_1, \lambda_2, \lambda_3\}$ denote the principal stretches. These inequalities ensure that the direction of greater stretch corresponds to the direction of greater stress. The inequalities lead to restrictions on the choice of the model, traditionally written as (Truesdell and Noll, 2004, p. 171):

$$\lambda_i^2 \lambda_i^2 \beta_1 > \beta_{-1}, \quad \text{if} \quad \lambda_i \neq \lambda_i,$$
 (44)

$$\lambda_i^4 \beta_1 \ge \beta_{-1}, \quad \text{if} \quad \lambda_i = \lambda_i,$$
 (45)

where the response functions for incompressible materials are given by

$$\beta_1 = 2W_1, \quad \beta_{-1} = -2W_2.$$
 (46)

These conditions, derived from the original inequalities, are crucial for ensuring the non-negativity of the work done by stresses during deformation. In the context of ideal shear, these inequalities ensure the expected behavior that the shear strains remain in the same direction as the applied shear force.

For SIMs, we have $\beta_1 = 0$, and we see that both inequalities (44)–(45) imply

$$\beta_{-1} < 0, \quad \Rightarrow \quad \frac{\partial W}{\partial I_2} > 0,$$
 (47)

which implies, from (18) that the Young modulus is also positive, as expected. These are the same conditions for the existence of a strain for a given stress (Nordenholz and O'Reilly, 1998).

Finally, we also comment on the so-called empirical inequalities (Truesdell and Noll, 2004, p. 171) given by

$$\beta_1 > 0, \ \beta_{-1} \le 0.$$
 (48)

As the name suggests, these inequalities are not based on first principles and are inspired by observations of rubber-like materials. They are used to ensure that the constitutive model predicts realistic responses under various loading conditions. In particular, they are sufficient to ensure that a tensile load leads to an extension, as expected (Batra, 1976). However, the empirical conditions are not necessary for this particular behavior as shown in Section 3.2.1. Further, it has also been established that these inequalities are not suitable for soft tissues (Mihai and Goriely, 2011). Hence it is no surprise that for SIMs the first inequality is not satisfied.

3.5. The Poynting effect

The Poynting effect in the context of simple shear deformations is defined as the occurrence of normal stresses in the direction perpendicular to the shear plane. When a material undergoes a simple shear deformation given by (26), the Cauchy stress tensor T may exhibit non-zero off-diagonal shear stress components and diagonal normal stress components (Billington, 1986; Poynting, 1909).

The Poynting effect refers to a situation where the normal stress components $T_{11} \neq T_{22}$. A positive Poynting effect is observed if $T_{22} < 0$, implying that the material experiences a compressive normal stress in the x_2 direction due to the shearing action, and the sheared faces of the material tend to 'spread apart'. Conversely, a negative Poynting effect (Horgan and Murphy, 2017; Mihai and Goriely, 2011) is characterized by $T_{22} > 0$, where a tensile normal stress develops in the x_2 direction, causing the sheared faces to 'draw together'.

The implication of the Poynting effect extends to the expected behavior under ideal shear stress, where the difference in shear stress $T = (\beta_1 - \beta_{-1})k$ is linked to either positive or negative Poynting effects.

For SIMs, we have from (47) that $T_{22} < 0$ in simple shear. Hence we conclude that all second-invariant materials exhibit the positive Poynting effect, which is not always observed for soft tissues (Destrade et al., 2015; Mihai et al., 2015) and suggests that such models may not be universally suitable for all such tissues.

4. Data analysis

The burgeoning field of automated model discovery presents a transformative approach to constitutive modeling, using the power of neural networks to decipher complex material behaviors from expansive datasets. Neural networks, in particular, have been identified as a robust tool for constitutive model discovery, capable of sifting through vast data troves to unearth models without a priori physical knowledge. Despite their prowess in data fitting, classical neural networks ignore the rich legacy of constitutive modeling (Holzapfel, 2001), at times disregarding thermodynamic principles and established physical laws. As a result, they often fail to extrapolate beyond their training regime. They excel at numerical fitting yet fall short in providing interpretative insights into the physics they model. Here we will use model discovery inspired by constitutive artificial neural networks (Linka et al., 2021a,b). These networks embed physics directly into the network architecture and discover models that are not only data-compliant but also physically grounded, especially when they are reverse-engineered from classical constitutive elements, trained on a diverse array of mechanical tests, and validated against the mechanical properties of soft tissues (Linka and Kuhl, 2023; Linka et al., 2023a,b; Pierre et al., 2023). As such, they offer an intuitive understanding and a clear physical interpretation of their parameters and provide an important step towards a truly autonomous discovery of physically motivated models (Taç et al., 2024; Peirlinck et al., 2024).

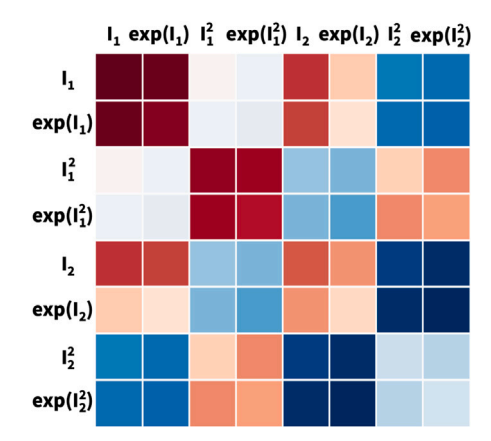


Fig. 4. Discovered best-in-class one- and two-term models for human brain. Discovered one-term models, on the diagonal, and two-term models, off-diagonal, for model discovery with eight terms. Models are made up of eight functional building blocks: linear, exponential linear, quadratic, and exponential quadratic terms of the first invariant, rows and columns one through four, and of the second invariant, rows and columns five through eight. The color code indicates the quality of fit to human brain data, ranging from dark blue, best fit, to dark red, worst fit.

Specifically, in pursuit of constitutive models that conform to the foundational principles of material behavior, we use a family models that inherently satisfy thermodynamic consistency, material objectivity (Truesdell and Noll, 2004), symmetry, incompressibility, constitutive restrictions, and polyconvexity (Antman, 2005),

$$W(I_{1}, I_{2}) = w_{1} [I_{1} - 3] + w_{2,2} [\exp(w_{1,2} [I_{1} - 3]) - 1] + w_{3} [I_{1} - 3]^{2} + w_{2,4} [\exp(w_{1,4} [I_{1} - 3]^{2}) - 1] + w_{5} [I_{2} - 3] + w_{2,6} [\exp(w_{1,6} [I_{2} - 3]) - 1] + w_{7} [I_{2} - 3]^{2} + w_{2,8} [\exp(w_{1,8} [I_{2} - 3]^{2}) - 1].$$

$$(49)$$

This family of models consists of eight terms and represents a total of $2^8 = 256$ different models with the twelve constant model parameters w_i and $w_{i,j}$. In particular, it includes the linear FIM (the classical neo-Hookean) and the Mooney–Rivlin models and many other popular existing models as special cases. We use uniaxial tension, uniaxial compression, and simple shear tests from human brain tissue of the gray matter cortex (Budday et al., 2017) to discover the model and parameters that best explain the experimental data (Linka et al., 2023a). This allows us to directly compare the performance of first- and second-invariant models (McCulloch et al., 2024).

Fig. 4 summarizes the discovered best-in-class one- and two-term models from all possible models in Eq. (49). Squares on the diagonal represent the eight one-term models: the linear, $[I_{1,2}-3]$, exponential linear, $\exp([I_{1,2}-3])-1$, quadratic, $[I_{1,2}-3]^2$, and exponential quadratic, $\exp([I_{1,2}-3]^2)-1$, models in terms of the first and second invariants, I_1 and I_2 , in rows and columns one through four and five through eight. Squares outside the diagonal represent the 28 two-term models with all possible combinations of any two of these eight terms. The color code indicates the quality of fit, ranging from dark blue for the best fit to dark red for the worst fit. We define the quality of fit as the remaining error after fitting the model to the data by minimizing the loss function that consists of the root mean squared error, the L_2 norm of the error between the model stresses and the experimentally measured stresses. Specifically, we consider n=17 stretch-stress data points in tension, compression, and shear, as indicated in Figs. 5 to 7 and scale each testing mode by the maximum stretch to weigh all three modes equally (Destrade et al., 2017).

Strikingly, for the best-in-class one-term models, all four second-invariant models outperform the four first-invariant models as we conclude from the blue-to-orange colors for the fifth to eights squares on the diagonal compared to the dark red colors for the first to fourth squares. Notably, the widely used neo-Hookean model, $W = w_1 [I_1 - 3]$, has the worst fit of all one-term models, followed by the popular Demiray model, $W = w_{2,2} [\exp(w_{1,2}[I_1 - 3]) - 1]$.

Figs. 5 and 6 illustrate the eight one-term FIMs and SIMs associated with the diagonal terms in Fig. 4 in terms of the nominal stress as a function of stretch or shear strain. All eight one-term models struggle to fit all three experiments simultaneously and overestimate the tensile stresses, while underestimating the compression and shear stresses. In agreement with Fig. 4, the second-invariant models in Fig. 6 provide a better fit to the data than the first-invariant models in Fig. 5.

Fig. 7 illustrates the discovered best-in-class two-term models associated with the dark blue of best-fit off-diagonal terms in Fig. 4 in terms of the nominal stress as a function of stretch or shear strain. We note a significantly improved fit compared to the one-term models in Figs. 5 and 6. The four best-in-class two-term models all combine the linear or exponential linear term $[I_2 - 3]$ or $\exp([I_2 - 3]) - 1$, with the quadratic or exponential quadratic term $[I_2 - 3]^2$ or $\exp([I_2 - 3]^2) - 1$, strikingly, all in terms of the second invariant. Notably, the widely-used Mooney–Rivlin model with linear terms in both invariants, $W = w_1 [I_1 - 3] + w_5 [I_2 - 3]$, is the third worst of all 28 two-term models. Taken together, the best-in-class two-term models in Fig. 7 confirm the trend of the one-term models in Figs. 5 and 6: For human brain tissue in tension, compression, and shear, second-invariant models perform significantly better than first-invariant models.

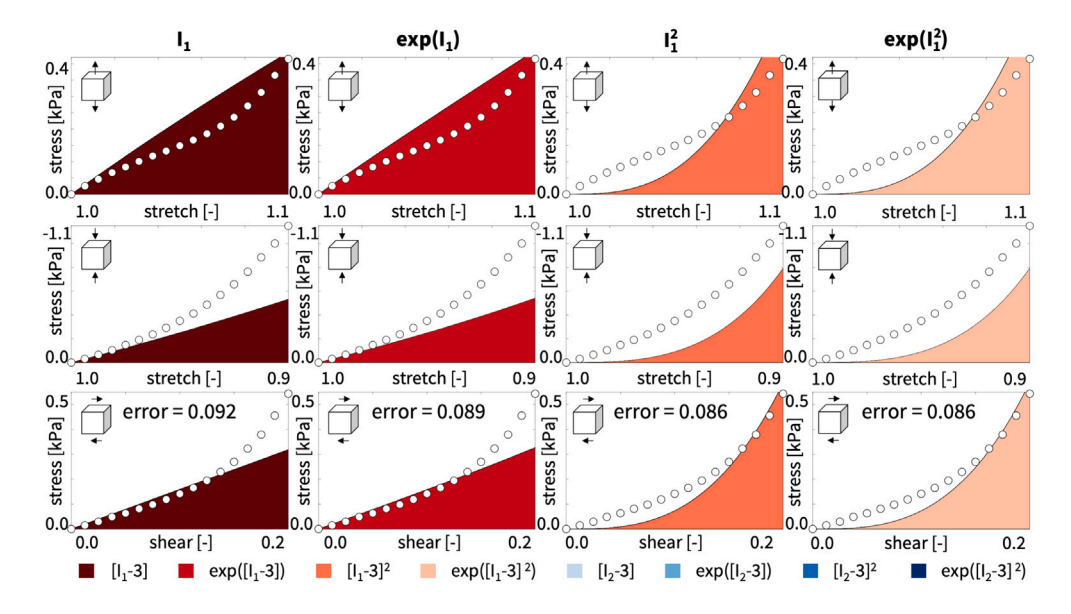


Fig. 5. Discovered one-term first-invariant models. Nominal stress as a function of stretch or shear strain for human gray matter tension, compression, and shear data. Circles represent the experimental data; color-coded regions represent the discovered terms for the linear, $W = [I_1 - 3]$, exponential linear, $W = \exp([I_1 - 3]) - 1$, quadratic, $W = [I_1 - 3]^2$, and exponential quadratic, $W = \exp([I_1 - 3]^2) - 1$, models; error value indicates the quality of fit, measured in the L_2 norm.

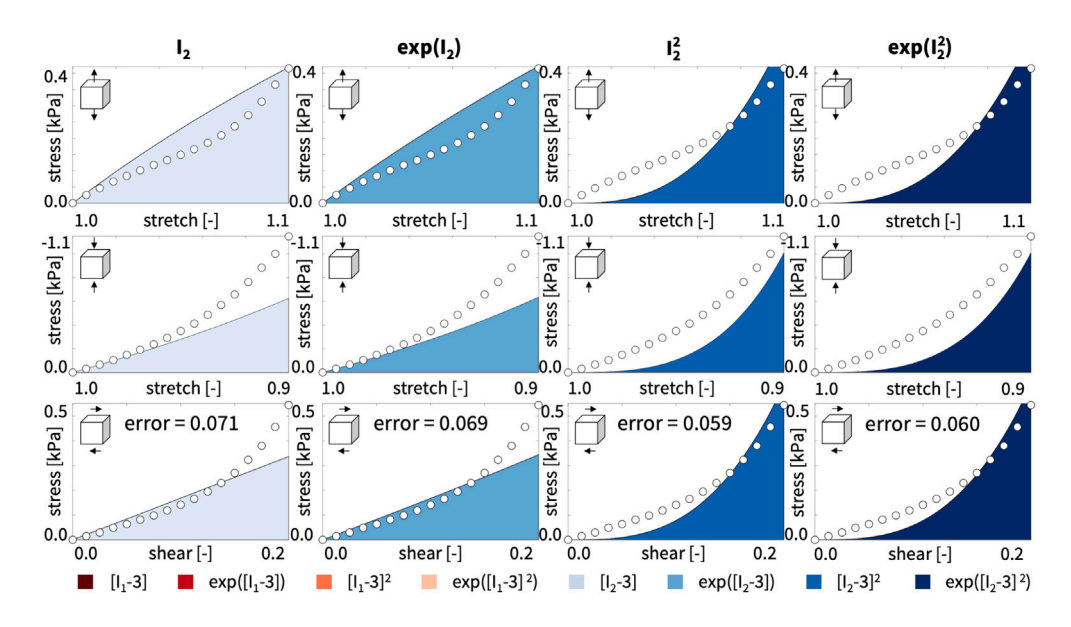


Fig. 6. Discovered one-term second-invariant models. Nominal stress as a function of stretch or shear strain for human gray matter tension, compression, and shear data. Circles represent the experimental data; color-coded regions represent the discovered terms for the linear, $W = [I_2 - 3]$, exponential linear, $W = \exp([I_2 - 3]) - 1$, quadratic, $W = [I_2 - 3]^2$, and exponential quadratic, $W = \exp([I_2 - 3]^2) - 1$, models; error value indicates the quality of fit.

Lastly, Fig. 8 illustrates the Poynting effect of the discovered best-in-class models for human brain. The top row highlights the best-in-class one-term models and the bottom row highlights the best-in-class two-term models. For all eight models, the load case of simple shear induces compressive stresses normal to the direction of shear. For models with linear terms, the Poynting effect is already visible at the zero-shear limit. For models with only quadratic terms, the Poynting has a horizontal tangent at the origin and only becomes visible for shear stresses on the order of 0.05. Importantly, none of the first-invariant models can capture the Poynting effect—only models that include the second invariant can display this characteristic behavior of lateral tension or compression when

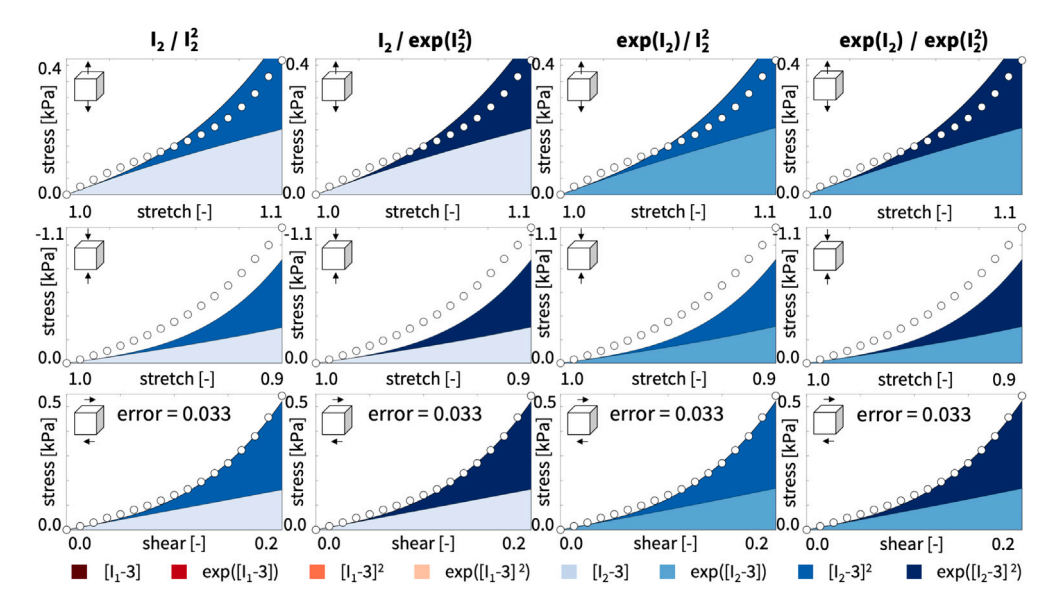


Fig. 7. Discovered best-in-class two-term models. Nominal stress as a function of stretch or shear strain for human gray matter tension, compression, and shear data. Circles represent the experimental data; color-coded regions represent the discovered model terms; error value indicates the quality of fit.

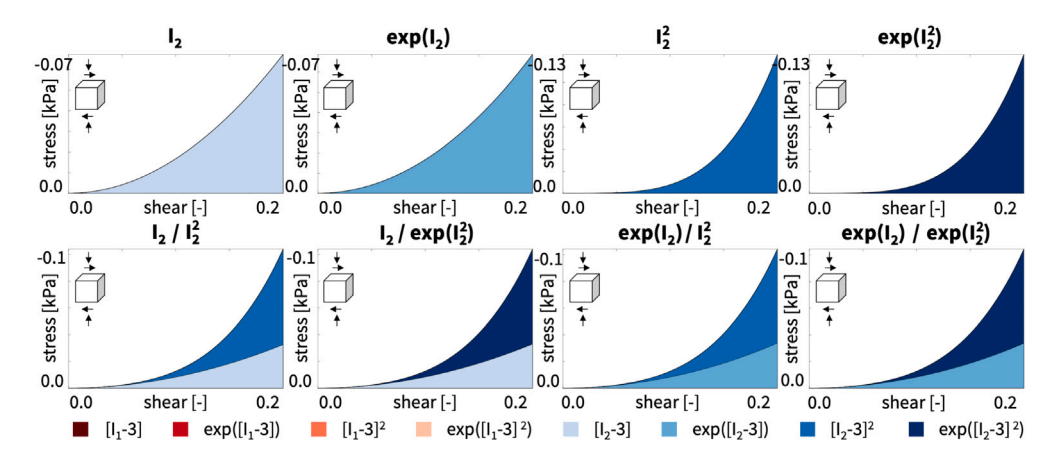


Fig. 8. Poynting effect for discovered best-in-class models. Normal stress as a function of shear strain for the best-in-class one-term models, top row, and best-in-class two-term models, bottom row, for human gray matter shear data. Color-coded regions represent the discovered model terms.

subjected to shear. Our algorithm automatically discovers second-invariant models for gray matter tissue, suggesting that this is a relevant feature of the human brain.

5. Conclusion

In the development of constitutive models for hyperelastic materials, the dependence on the first and second invariants I_1 and I_2 has been inspired by the statistical mechanics of long-chain molecules. Early neo-Hookean models, derived from the assumption of Gaussian statistics of chain configurations, were limited to terms dependent only on the first invariant I_1 . However, we now increasingly recognize that this term alone cannot adequately describe the experimentally observed material behavior, especially under finite deformations.

The introduction of I_2 -dependent terms was motivated by the need to account for non-affine deformations of the molecular chains, which the classical Gaussian models could not capture. Microscopically, in non-affine deformations, chains do not deform uniformly with the macroscopic strain, a situation commonly encountered in polymeric networks. Inclusion of the second invariant allows for the modeling of constraints imposed by neighboring chains and the resultant restriction on the non-affine deformation of the chains, a concept supported by the tube model of polymer dynamics. Hence, in addition to variations in chain length, these models also include variations of cross-sectional chain area. Macroscopically, the second invariant proves necessary to capture the

well-known Poynting effect. From a theoretical point of view, second-invariant models also offer the possibility of new semi-inverse solutions, an avenue of research that is completely open (Goodbrake et al., 2020).

Clearly, second-invariant models suffer from the same limitations as first-invariant models. Both naturally give rise to universal relations that are unlikely to be met exactly by real-life materials. This is not necessarily a fundamental problem and these universal relations can be used as a different way to measure goodness of fit for either types of model. Second, restricting to a single invariant also implies that some qualitative phenomena cannot be properly taken into account. For instance, first-invariant models do not exhibit the Poynting effect while second-invariant always exhibit a positive effect, neither of which may be reflected on the behavior of particular materials.

Nevertheless, our study shows that, for human brain tissue, second-invariant models consistently outperform first-invariant models, both for best-in-class one-term and two-term models. This suggests that the second invariant plays a much more significant role than previously assumed. This observation is not limited to brain data. A recent model-discovery study on human cardiac tissue using similar methods shows that the isotropic part of the strain-energy function is also best described by second-invariant models (Martonova et al., 2024). Therefore, including the second invariant generates a much richer base of potential candidate terms for constitutive models. This provides compelling new models, either as combined first- and second-invariant models in the spirit of Mooney and Rivlin or as entirely stand alone second-invariant models.

CRediT authorship contribution statement

Ellen Kuhl: Writing – review & editing, Writing – original draft, Visualization, Validation, Supervision, Software, Resources, Project administration, Methodology, Investigation, Funding acquisition, Formal analysis, Data curation, Conceptualization. Alain Goriely: Writing – review & editing, Writing – original draft, Visualization, Validation, Supervision, Software, Resources, Project administration, Methodology, Investigation, Funding acquisition, Formal analysis, Data curation, Conceptualization.

Declaration of competing interest

We declare that there is no conflict of interest concerning our research, findings, and publication of this work.

Data availability

The authors do not have permission to share data.

Acknowledgments

It is our great pleasure to acknowledge helpful discussion and expertise from Giuseppe Saccomandi. We would also like to thank both not-so-anonymous reviewers for their suggestions. This work has been funded by the NSF grant CMMI 2318188. Alain Goriely is grateful for the hospitality of the Mathematics Department at Stanford where this work was carried out. The I-too- \P - I_2 movement started on 24 February at Il Fornaio, Palo Alto, and is now, very slowly, taking the world by storm.

References

Alibakhshi, Amin, Imam, Ali, Haghighi, Shahram Etemadi, 2021. Effect of the second invariant of the Cauchy–Green deformation tensor on the local dynamics of dielectric elastomers. Int. J. Non-Linear Mech. 137, 103807.

Anssari-Benam, Afshin, Bucchi, Andrea, Saccomandi, Giuseppe, 2021. On the central role of the invariant I_2 in nonlinear elasticity. Internat. J. Engrg. Sci. 163, 103486.

Anssari-Benam, Afshin, Horgan, Cornelius O., 2021. On modelling simple shear for isotropic incompressible rubber-like materials. J. Elasticity 147 (1), 83–111. Anssari-Benam, Afshin, Horgan, Cornelius O., 2022. A three-parameter structurally motivated robust constitutive model for isotropic incompressible unfilled and filled rubber-like materials. Eur. J. Mech. A Solids 95, 104605.

Antman, S.S., 2005. Nonlinear Problems of Elasticity. Springer New York.

Aydogdu, A.B., Loos, K., Johlitz, M., Lion, A., 2021. A new concept for the representative directions method: Directionalisation of first and second invariant based hyperelastic models. Int. J. Solids Struct. 222, 111017.

Batra, R.C., 1976. Deformation produced by a simple tensile load in an isotropic elastic body. J. Elasticity 6 (1), 109-111.

Beatty, M.F., 1987. A class of universal relations in isotropic elasticity theory. J. Elasticity 17 (2), 113-121.

Beatty, Millard F., 2003. An average-stretch full-network model for rubber elasticity. J. Elasticity 70, 65-86.

Billington, E.W., 1986. The poynting effect. Acta Mech. 58 (1), 19-31.

Blatz, P.J., Ko, W.L., 1962. Application of finite elasticity to the deformation of elastic materials. Trans. Soc. Rheol. 6, 227-251.

Budday, S., Sommer, G., Birkl, C., Langkammer, C., Haybaeck, J., Kohnert, J., Bauer, M., Paulsen, F., Steinmann, P., Kuhl, E., et al., 2017. Mechanical characterization of human brain tissue. Acta Biomater. 48, 319–340.

Destrade, M., Horgan, C.O., Murphy, J.G., 2015. Dominant negative Poynting effect in simple shearing of soft tissues. J. Engrg. Math. 95, 87-98.

Destrade, Michel, Murphy, Jerry G., Saccomandi, Giuseppe, 2012. Simple shear is not so simple. Int. J. Non-Linear Mech. 47 (2), 210-214.

Destrade, Michel, Saccomandi, Giuseppe, Sgura, Ivonne, 2017. Methodical fitting for mathematical models of rubber-like materials. Proc. R. Soc. A 473 (2198), 20160811.

Ehret, Alexander Edmund, Stracuzzi, Alberto, 2022. Variations on Ogden's model: close and distant relatives. Phil. Trans. R. Soc. A 380 (2234), 20210322. Fried, Eliot, 2002. An elementary molecular-statistical basis for the Mooney and Rivlin–Saunders theories of rubber elasticity. J. Mech. Phys. Solids 50 (3), 571–582.

Fu, Y.B., Ogden, R.W., 2001. Nonlinear Elasticity. Theory and Applications. Cambridge University Press, Cambridge.

Goodbrake, Christian, Yavari, Arash, Goriely, Alain, 2020. The anelastic Ericksen problem: Universal deformations and universal eigenstrains in incompressible nonlinear anelasticity. J. Elasticity, 142 (2), 291–381.

Goriely, A., 2017. The Mathematics and Mechanics of Biological Growth. Springer Verlag, New York.

Hill, James M., 1973. Partial solutions of finite elasticity-three dimensional deformations. Z. Ang. Math. Phys. ZAMP 24, 609-618.

Holzapfel, G.A., 2001. Biomechanics of soft tissue. In: The Handbook of Materials Behavior Models, vol. 3, pp. 1049-1063.

Horgan, C.O., Murphy, J.G., 2017. Poynting and reverse Poynting effects in soft materials. Soft Matter 13 (28), 4916-4923.

Horgan, Cornelius O., Smayda, Michael G., 2012. The importance of the second strain invariant in the constitutive modeling of elastomers and soft biomaterials. Mech. Mater. 51, 43–52.

Kearsley, E.A., 1989. Note: Strain invariants expressed as average stretches. J. Rheol. 33 (5), 757-760.

Kumar, Gordon, Brassart, Laurence, 2023. On tube models of rubber elasticity: fitting performance in relation to sensitivity to the invariant I_2 . Mech. Soft Mater. 5 (1), 6.

Linka, Kevin, Hillgärtner, Markus, Abdolazizi, Kian P., Aydin, Roland C., Itskov, Mikhail, Cyron, Christian J., 2021a. Constitutive artificial neural networks: A fast and general approach to predictive data-driven constitutive modeling by deep learning. J. Comput. Phys. 429, 110010.

Linka, Kevin, Kuhl, Ellen, 2023. A new family of constitutive artificial neural networks towards automated model discovery. Comput. Methods Appl. Mech. Engrg. 403, 115731.

Linka, Kevin, Pierre, Sarah R. St, Kuhl, Ellen, 2023a. Automated model discovery for human brain using constitutive artificial neural networks. Acta Biomater. 160, 134–151.

Linka, Kevin, Reiter, Nina, Würges, Jasmin, Schicht, Martin, Bräuer, Lars, Cyron, Christian J., Paulsen, Friedrich, Budday, Silvia, 2021b. Unraveling the local relation between tissue composition and human brain mechanics through machine learning. Front. Bioeng. Biotechnol. 9, 704738.

Linka, Kevin, Tepole, Adrian Buganza, Holzapfel, Gerhard A., Kuhl, Ellen, 2023b. Automated model discovery for skin: Discovering the best model, data, and experiment. Comput. Methods Appl. Mech. Engrg. 410, 116007.

Lopez-Pamies, Oscar, 2010. A new I_2 -based hyperelastic model for rubber elastic materials. Compt. R. Mecanique 338 (1), 3–11.

Martonova, Denisa, Peirlinck, Mathias, Linka, Kevin, Holzapfel, Gerhard A., Leyendecker, Sigrid, Kuhl, Ellen, 2024. Gerhard a holzapfel sigrid leyendecker ellen kuhl automated model discovery for human cardiac tissue: Discovering the best model and parameters. bioRxiv, 2024–02.

McCulloch, J.A., Pierre, S.R. St., Linka, K., Kuhl, E., 2024. On sparse regression, L_p-regularization, and automated model discovery. Internat. J. Numer. Methods Engrg. http://dx.doi.org/10.1002/nme.7481.

Miehe, C., Göktepe, S., Lulei, F., 2004. A micro-macro approach to rubber-like materials—part I: the non-affine micro-sphere model of rubber elasticity. J. Mech. Phys. Solids 52 (11), 2617–2660.

Mihai, L. Angela, Chin, LiKang, Janmey, Paul A., Goriely, Alain, 2015. A comparison of hyperelastic constitutive models applicable to brain and fat tissues. J. R. Soc. Interface 12 (110), 20150486.

Mihai, L.A., Goriely, A., 2011. Positive or negative poynting effect? the role of adscititious inequalities in hyperelastic materials. Proc. Roy. Soc. Lond. A 467 (2136), 3633–3646.

Mihai, L.A., Goriely, A., 2012. Numerical simulation of shear and the poynting effects by the finite element method: An application of the generalised empirical inequalities in non-linear elasticity. Int. J. Non-Linear Mech. 49, 1–14.

Moon, H., Truesdell, C., 1974. Interpretation of adscititious inequalities through the effects pure shear stress produces upon an isotropic elastic solid. Arch. Ration. Mech. Anal. 55 (1), 1–17.

Mooney, Melvin, 1940. A theory of large elastic deformation. J. Appl. Phys. 11 (9), 582-592.

Nordenholz, Thomas R., O'Reilly, Oliver M., 1998. On the existence of a stretch for a prescribed stress in isotropic, incompressible elastic materials. Math. Mech. Solids 3 (2), 169–181.

Ogden, R.W., 1984. Non-Linear Elastic Deformations. Dover, New york.

Peirlinck, Mathias, Linka, Kevin, Hurtado, Juan A., Kuhl, Ellen, 2024. On automated model discovery and a universal material subroutine for hyperelastic materials. Comput. Methods Appl. Mech. Engrg. 418, 116534.

Pierre, Sarah R. St, Linka, Kevin., Kuhl, Ellen., 2023. Principal-stretch-based constitutive neural networks autonomously discover a subclass of Ogden models for human brain tissue. Brain Multiphysics 4, 100066.

Poynting, John Henry, 1909. On pressure perpendicular to the shear planes in finite pure shears, and on the lengthening of loaded wires when twisted. Proc. R. Soc. Lond. Series A, Contain. Pap. Math. Phys. Char. 82 (557), 546–559.

Pucci, E., Saccomandi, G., 1997. On universal relations in continuum mechanics. Contin. Mech. Therm. 9 (2), 61-72.

Puglisi, G., Saccomandi, G., 2016. Multi-scale modelling of rubber-like materials and soft tissues: an appraisal. Proc. R. Soc A 472 (2187), 20160060.

Rivlin, R.S., 1948. Large elastic deformations of isotropic materials. IV. further developments of the general theory. Philos. Trans. Roy. Soc. A 241 (835), 379–397. Saccomandi, G., 2001. Universal results in finite elasticity. Nonlinear Elast. Theory Appl. 283, 97.

Taç, Vahidullah, Linka, Kevin, Sahli-Costabal, Francisco, Kuhl, Ellen, Tepole, Adrian Buganza, 2024. Benchmarking physics-informed frameworks for data-driven hyperelasticity. Comput. Mech. 73 (1), 49–65.

Treloar, Leslie R.G., 1944. Stress-strain data for vulcanized rubber under various types of deformation. Rubber Chem. Technol. 17 (4), 813-825.

Truesdell, C., Noll, W., 2004. The Non-Linear Field Theories of Mechanics. Springer.